On the Effect of Non-Raining Parameters in Retrieval of Surface Rain Rate Using TRMM PR and TMI Measurements

Srinivasa Ramanujam, Chandrasekar Radhakrishnan, Deepak Subramani, and Balaji Chakravarthy

***Abstract*—Microwave radiation with the inherent advantage of its ability to partially penetrate clouds is ideally suited for remote measurements of precipitation, especially over the oceanic regions. The retrieval problem is of great practical interest, as precipitation over the oceans has to be necessarily remotely sensed. More importantly, precipitation is also a crucial input in many weather and climate models. A downward looking space borne radiometer such as the TRMM's Microwave Imager (TMI), however, does not sense the surface rain fall directly. Rather, it measures the upwelling radiation coming from the top-of-atmosphere which depends on the total quantities of the parameters that can affect the radiation in the chosen frequency range. In addition to precipitation, the attenuation and augmentation of total cloud content and integrated precipitable water content by absorption and emission, respectively, affect the microwave brightness temperatures in various frequencies. In the present work, a systematic study has been conducted to investigate the effect of total cloud and precipitable water contents on surface rainrate retrievals from the TMI measured brightness temperatures (BT). While a Bayesian framework is used to assimilate radar reflectivities into hydrometeor structures, a neural network is used to correlate rain and cloud parameters with brightness temperatures. The correlation between the TMI brightness temperatures and the TRMM's Precipitation Radar (TRMM-PR) is used as the benchmark for comparison. A community developed software meso-scale Weather Research and Forecast (WRF) is used to simulate the cloud and precipitable water content, along with the surface rainfall rate for several rain events in the past. Four cases are considered: (a) TRMM PR's near surface rain rate is correlated with TMI brightness temperatures directly; (b) the total cloud and precipitable water contents along with surface rainfall simulated using WRF are correlated with TMI BTs; (c) similar to case (b) with near surface rainfall taken from TRMM PR measurements; (d) total cloud and precipitable water contents and the surface rain rate are corrected with PR vertical reflectivity profile in a Bayesian framework. The freely available QuickBeam software has been used for simulation of reflectivities at the TRMM PR frequency. The corrected data are then correlated with TMI BTs. Results show that surface rain fall retrievals can be radically improved by using TRMM PR vertical rain corrected total cloud and precipitable water content.**

***Index Terms*—Artificial neural network, Bayesian inference, microwave remote sensing, quickbeam, rainfall retrieval algorithm, TRMM satellite, WRF.**

Manuscript received September 24, 2011; accepted February 13, 2012. Date of publication April 10, 2012; date of current version June 28, 2012.

The authors are with the Indian Institute of Technology Madras, Chennai 600 036, India.

Color versions of one or more of the figures in this paper are available online at http://ieeexplore.ieee.org.

Digital Object Identifier 10.1109/JSTARS.2012.2189557

I. Introduction

REMOTE sensing of earth's atmosphere in the microwave spectrum of radiation, with the inherent advantage of its ability to partially penetrate clouds, is an ideal method of obtaining a global rainfall map. The latter has several practical applications such as (a) short term-flood estimation, agricultural productivity, underground water level control, and (b) long term estimation, which serves as input to the climatological models. The radiometer aboard the recent successful program by NASA and Japan's space agency JAXA, the Tropical Rainfall Measuring Mission, called as TRMM's Microwave Imager (TMI) has taken unprecedented satellite images of earth's weather for the past 14 years. A description of the TRMM's instrument and its characteristics can be found in Kummerow *et al.* [1].

The key rain measuring instruments of the TRMM satellite are the TRMM's Microwave Imager (TMI), the TRMM's Precipitation Radar (TRMM PR) and the Visible and Infra Red Scanner (VIRS). Of the three instruments aboard the TRMM, the TMI and TRMM-PR are based on microwave radiances, and have the ability to penetrate clouds partially to make measurements of cloud and rainfall structure. The combination of a space borne radar and radiometer on the same space platform has enabled many researchers to develop combined rainfall retrieval algorithms [2]–[4].

Though the TMI and TRMM PR are on the same platform and hence "see" the same rain scene, the underlying physics between the two instruments are different. While the TRMM PR can detect the signal from precipitating water and ice particles, the multi frequency dual polarized TMI sensor can detect cloud and precipitating contents, in addition to the attenuation due to precipitable water in the atmosphere.

The operational geophysical data products retrieved from TMI sensor include vertical profiles of hydrometeors, *viz.*, cloud liquid water, cloud ice, precipitating water and precipitating ice. The retrieval algorithm of TMI rain data products uses a Bayesian framework, powered by *a priori* data base generated using the Goddard Cumulus Ensemble (GCE) model and a one dimensional plane parallel radiative transfer model to simulate the brightness temperatures [5].

While the total cloud content can be obtained by vertically integrating the retrieved cloud profiles, precipitable water content which is a crucial hydrological parameter in numerical weather forecasting models is not available in the operational data products.

1939-1404/$31.00 © 2012 IEEE

Since the radiometer measures the brightness temperatures that are affected by the total cloud and precipitable contents, an algorithm to estimate precipitation should consider total cloud content and precipitable water contents as well.

Czekala [6] has found that a given liquid water path can result in different values of brightness temperatures depending on the amount of rain water present in the cloud. Hence, in order to ensure physical consistency in the retrieved products, the geophysical parameters should be retrieved simultaneously.

Auria *et al.* [7] used a cloud database from a microphysical cloud model [8] to estimate the surface rainfall from simulated microwave brightness temperatures corresponding to the SSMI sensor. In order to improve on the accuracy, the authors divided the cloud database into five clusters of 5000 profiles. The results showed that the clustered database can estimate surface rain rate with a low RMSE value of 1.87 mm/hr for minimum mean square technique using rain rate as the single parameter, while the RMSE for estimation of rain rate using retrieval of complete vertical structure is 6.27 mm/hr.

An algorithm for determining the cloud liquid water and precipitable water content during the monsoon period using ground based radiometer observations over New Delhi region was developed by Bhattacharya and Uppal [9]. The authors have found that the poor cross correlation between cloud liquid water path and the precipitable water content based on radiosonde measurements of about 0.4 allows them to estimate the parameters simultaneously treating them as independent, while developing the retrieval algorithm. Their retrieval results show that the cloud liquid water path can be retrieved with an accuracy of about 10% to 20%, while the precipitable water content with an accuracy of about 7% to 14%, both with respect to an independent radiosonde measurement over the Arabian Sea.

A need for accurate retrieval of precipitable water which is critical for radiative transfer modeling, and for specifying advective forcing for cloud resolving models has motivated Turner *et al.* [10] to develop a regression based retrieval algorithm to simultaneously estimate the liquid water path and the precipitable water content. The database is generated from radiosonde measurements, and the brightness temperatures are obtained by using the monoRTM as the forward model.

Sanchez *et al.* [11] used a cloud resolving model to generate cloud liquid water path (CLWP), rain water path (RWP) and ice water path (IWP). The rain rate is then retrieved by regressing the linear equation

$$RR = a_0 + a_1 CLWP + a_2 RWP + a_3 IWP \qquad (1)$$

in which the parameters a_0, a_1, a_2 and a_3 were obtained from regression analysis. The Microwave Integrated Retrieval Scheme, a sensor independent scheme, was used to retrieve the cloud, rain and ice water paths.

Weinman *et al.* [12] developed an algorithm to retrieve precipitation profiles using combined radar-radiometer measurements. Measurements from 1985–86 CRL/NASA rain measuring experiment from airborne X and Ka band radars and X band passive radiometer over the Atlantic Ocean were used to develop the algorithm.

Based on the literature survey, systematic studies on the effect of total cloud and precipitable water content that affects both the radar and radiometer signals are scarce. This is a prime motivation for the present work.

In the present study, a neural network based retrieval algorithm is proposed to retrieve the surface rain rate from TMI brightness temperatures. The correlation between TRMM PR's near surface rain rate with TMI Brightness Temperatures (BTs) is used as the benchmark for comparison. The following four cases are considered: (a) TRMM PR's near surface rain rate is correlated with TMI brightness temperatures; (b) the total cloud and precipitable water contents along with surface rainfall simulated using WRF are correlated with TMI BTs; (c) case (b) with near surface rainfall taken from TRMM PR measurements; (d) total cloud and precipitable water contents and the surface rain rate are corrected with PR vertical reflectivity profile in a Bayesian framework. The non-commercial radar simulation package "QuickBeam" has been used for simulation of reflectivities at 13.8 GHz corresponding to the TRMM PR frequency. The "corrected" hydrometeor structure is then used to correlate the rain products with TMI BTs.

II. Weather Research and Forecasting Model (WRF)

The mesoscale community developed Weather Research and Forecasting (WRF) model has been used for obtaining the vertical atmospheric profiles of the raining atmosphere. For this purpose, 31 snapshots of 14 cyclones that originated in the North Indian Oceanic region between 2003 and 2010 have been considered. Out of the 31 snapshots, 14 are taken from cyclones that evolved in the Arabian Sea waters bounded by 0° to 20° N and 50° to 70° E, while the remaining 17 snapshots were taken from the snapshots of cyclones that originated in the Bay of Bengal waters bounded between 5° to 25° N and 80° to 100° E. Several snapshots of the same cyclone in its birth, growth and mature phase are taken based on TRMM satellite overpasses.

The input profiles are generated for the snapshots of rainy pixels "seen" by the Tropical Rainfall Measuring Mission (TRMM) satellite. Table I shows details of the snapshots considered, and the corresponding TRMM orbit number.

The Advanced Research WRF (ARW) mesoscale model WRFV3.1 has been used in the present study to generate the transient vertical profiles of temperature, humidity and cloud structures by solving the appropriate equations for flow, heat and mass transfer in the three dimensional atmosphere.

The ARW model solves the following governing equations:

1) continuity equation;
2) conservation of momentum;
3) conservation of energy;
4) equation of state.

The ARW dynamics solver integrates the compressible, nonhydrostatic Euler equations. Following Ooyama [13], the equations are cast in flux form using variables that have conservation properties.

The ARW model uses the traditional vertical σ coordinate system

$$\eta = (p_h - p_{ht})/\mu \qquad (2)$$

TABLE I
DETAILS OF SNAPSHOTS OF CYCLONES CONSIDERED IN PRESENT STUDY

Cyclone	TRMM orbit no	Lat bound	Lon bound
2003_01B	31283	10N - 20N	80E - 90E
2003_01B	31329	10N - 20N	80E - 90E
2003_02A	34175	0N - 10N	50E - 60E
2003_02A	34184	0N - 10N	50E - 60E
2004_Agni	40128	0N - 10N	50E - 70E
2004_Agni	40137	0N - 10N	50E - 70E
2005_Fanoos	45921	5N - 20N	85E - 95E
2006_Mala	48119	10N - 20N	85E - 95E
2006_Mala	48140	10N - 20N	85E - 95E
2006_Mala	48155	10N - 20N	85E - 95E
2007_Gonu	54399	10N - 20N	60E - 75E
2007_Gonu	54409	15N - 20N	60E - 70E
2007_Gonu	54414	15N - 25N	60E - 70E
2007_Gonu	54425	17N - 25N	60E - 75E
2007_Gonu	54470	10N - 20N	60E - 70E
2007_Sidr	56917	5N - 15N	85E - 95E
2007_Sidr	56926	5N - 15N	85E - 95E
2007_Sidr	56932	7N - 17N	85E - 95E
2007_Sidr	56947	10N - 20N	85E - 95E
2007_Sidr	56957	10N - 20N	85E - 95E
2008_Nargis	59527	5N - 15N	80E - 90E
2008_Nargis	59552	5N - 20N	80E - 90E
2008_Nargis	59588	5N - 20N	85E - 95E
2008_Nargis	59603	10N - 20N	90E - 100E
2010_Laila	71219	8N - 17N	83E - 95E
2010_Phet	71449	10N - 20N	55E - 70E
2010_Phet	71459	10N - 20N	55E - 65E
2010_Phet	71464	10N - 20N	55E - 65E
2010_Giri	73676	15N - 20N	90E - 95E
2010_Jal	73915	5N - 15N	80E - 85E
2010_Jal	73921	5N - 15N	80E - 85E

where

$$\mu = p_{hs} - p_{ht}. \tag{3}$$

p_h refers to the hydrodynamic component of the pressure, p_{hs} and p_{ht} refer to values for the dry atmosphere at the surface and top of the boundaries respectively.

p_{ht} remains constant and η decreases monotonically from a value of 1 at the surface and 0 at upper boundary of the model domain.

The flux form of the Euler equations with vertical σ coordinate system are expressed as

$$U_t + (\nabla.Vu) + p_x(p,\phi) = F_U, \tag{4a}$$
$$V_t + (\nabla.Vv) + p_y(p,\phi) = F_V, \tag{4b}$$
$$W_t + (\nabla.Vw) + p_\eta(p,\mu) = F_W, \tag{4c}$$
$$\Theta_t + (\nabla.V) = F_\Theta, \tag{4d}$$
$$\mu_t + (\nabla.V) = 0, \tag{4e}$$
$$\phi_t + \mu^{-1}\left[(V.\nabla\phi) - gW\right] = 0, \tag{4f}$$

where μ(x, y) represents the mass of the dry air per unit area within the column in the model domain at (x, y), U, V and W respectively represent the wind velocity vector components along the x, y, and z axes, respectively.

The terms F_U, F_V, F_W and F_θ appearing on the right-hand side of (4a)–(4d) represent the forcing terms arising from model physics, turbulent mixing, spherical projections, and the earth's rotation, respectively.

The suffix t that appears in (4a)–(4f) denotes the time derivative of the parameter. The variables in flux form are expressed as

$$U = \mu u/m \tag{5}$$
$$V = \mu v/m \tag{6}$$
$$W = \mu w/m \tag{7}$$
$$\Omega = \mu\eta/m \tag{8}$$

where m is the map-scale factor for mapping the equations to the sphere as

$$m = \frac{(\Delta x, \Delta y)}{\text{distance on the earth}}. \tag{9}$$

Finally, the equation of state is given by

$$p = p_0\left(\frac{R_d\theta}{p_o\alpha}\right)^\gamma. \tag{10}$$

The moisture and perturbation form of governing equations are described in detail by [14].

The Euler equations in flux form are solved numerically using a third-order Runge–Kutta scheme. The prognostic variables in the ARW solver are defined as $\Phi = (U, V, W, \Theta, \Phi', \mu', Q_m)$, while the model equations are defined as $\Phi_t = R(\Phi)$. The third-order Runge–Kutta scheme solves the equation in three steps in order to obtain a solution at $\Phi(t + \Delta t)$ from $\Phi(t)$ as:

$$\Phi^* = \Phi^t + \frac{\Delta t}{3}R(\Phi^t) \tag{11a}$$
$$\Phi^{**} = \Phi^t + \frac{\Delta t}{2}R(\Phi^*) \tag{11b}$$
$$\Phi^{t+\Delta t} = \Phi^t + \Delta t R(\Phi^{**}) \tag{11c}$$

where Δt is the discretized time step.

The time split integration scheme, spatial, advection (flux divergence) discretization, Courant number, a non-dimensional number that limits the stability constraints for the third-order Runge–Kutta scheme are detailed in [15].

The initial and boundary conditions used by the ARW model are taken from the National Center of Environmental Prediction (NCEP)'s final analysis (FNL) data. The FNL data are available at every six hours interval at one degree resolution ($\sim$ 100 km) and 28 vertical levels. The model domain considered in the present study is bounded as per the coordinates specified in the Table I. The vertical profiles are generated at a spatial resolution of 6 km$\times$6 km.

Table II shows the set of physics options used for executing the WRF. These physics options are chosen based on a sensitivity study conducted on Cyclone Jal, a category 1 cyclone that made its landfall near Chennai in 2010 [16].

TABLE II
PHYSICS OPTIONS USED FOR WRF SIMULATIONS

Cumulus parameterization	Grell-Devenyi ensemble scheme (GD)
Plantary Boundary Layer	Mellor-Yamada-janjic (Eta) TKE scheme (MYJ)
Microphysics	WRF Single Moment 3-class simple ice scheme (WSM3)
Surface layer physics	Monin-Obukhov (janjic Eta) scheme (JAN)
Land surface model	Pleim-Xu scheme (PLEIM)
Longwave Radiation Physics	Rapid Radiative Transfer Model (RRTM)
Shortwave Radiation Physics	Rapid Radiative Transfer Model for Global (RRTMG)

III. TRMM DATA PRODUCTS

For the present study, data from two rain measuring instruments, the TRMM's Microwave Imager and TRMM's Precipitation Radar are considered.

A. TRMM's Precipitation Radar

The TRMM PR's is an active instrument on board the TRMM that measures the reflectivity profiles at 13.8 GHz frequency. The nadir viewing sensor makes a horizontal spatial resolution of about 5 km at nadir, and measures reflectivity at every 250 m vertical, up to 20 km.

The TRMM PR's data products include the attenuation corrected reflectivity at 80 vertical levels, vertical rain profile at 80 levels, near surface rain, sigma zero, integrated path attenuation, freezing level, and bright band characteristics. The near surface rain is measured at the clutter free bin from the surface level. For the present study, the vertical rain, reflectivity profiles and the near surface rain data are taken from 2A25 data [17].

B. TRMM's Microwave Imager (TMI)

The TMI is a passive instrument that measures the upwelling brightness temperature emerging out of the top-of-atmosphere, after passing through an emitting, absorbing and scattering atmosphere. TMI measures brightness temperatures at microwave frequencies: 10.65 GHz, 19 GHz, 21 GHz, 37 GHz and 85 GHz. But for the 21 GHz channel that measures only the vertical polarization, all other channels measure the upwelling radiation from the top of atmosphere (TOA) in both vertical and horizontal polarizations.

The 1B11 data [17] which gives the brightness temperatures measured at effective field of view (EFOV) resolution is considered in the present study. The horizontal spatial resolution varies with frequency from 5 km$\times$7 km for 85 GHz to 10 km$\times$63 km for 10 GHz. Linear interpolation is done to increase the resolution of low frequency channels to match with 85 GHz channel resolution along the cross track direction.

IV. COLLOCATION STRATEGY

The present study uses the minimum distance strategy to identify the corresponding matching pixel to form a collocated data base. Spatial or volume based interpolations are not used in order to work with raw data at the available sensor resolution to the extent possible. Collocation is done at two levels.

A. Collocation of PR on TMI Pixels

The geolocation data from the TRMM PR and TMI data set is used as the basis for collocating PR pixels on TMI pixels. The distance between each of the TMI pixels from a given PR pixel is calculated using

$$d_j = \sqrt{(lat_{PR} - lat_{TMI,j})^2 + (lon_{PR} - lon_{TMI,j})^2} \quad (12)$$

where j refers to the jth TMI pixel. The minimum of d_j is used to find the matching TMI pixel for that PR pixel. In order to account for the shorter PR swath, the condition that the minimum distance should also be smaller than $0.01^\circ \sim 1$ km is posed. The collocated data base consists of matching TMI brightness temperatures for corresponding PR rain products.

B. Collocation of TRMM on WRF Pixels

The matching geolocation data from TMI, PR collocated data set is collocated with the geoinformation available with the WRF simulations. The distance formula mentioned in (12) is used for determining the matching WRF pixel for a given TRMM pixel. A tolerance of 0.01° has been set in this case as well. The final data set contains the rain and reflectivity information from the TRMM PR, pressure, temperature, relative humidty, cloud and rain water mixing ratios from WRF, and the corresponding brightness temperatures from the TMI.

V. ARTIFICIAL NEURAL NETWORK (ANN)

Artificial neural networks (ANNs) are found to be useful tools in mimicking the inputs and outputs which has a complex and nonlinear relationship from a given database. A neural network is defined based on its architecture, and consists of several layers. The first layer is the input layer, and the last layer is the output layer, while the intermediate layers which are hidden from the end user are called as hidden layers.

The input and output layer consist of a number of neurons equal to the number of input and output parameters, respectively. However, there is no general way of arriving at the number of hidden layers, or the number of neurons in each hidden layer. In the present study, neural network architecture with single hidden layer has been considered. The number of neurons in the single hidden layer is determined by conducting a neuron independence study.

The input and target data are normalized with respect to their minimum and maximum values using

$$x_{\text{norm}} = \frac{x - x_{\min}}{x_{\max} - x_{\min}} \quad (13)$$

where x is the input/output parameter, and the values of x_{norm} lie between 0 and 1.

A supervised neural network that makes use of known target values consists of two phases; the first phase is known as the training phase wherein the network is trained to mimic the known output. In this phase, the weights that connect the input and output neurons through the hidden layers are iteratively updated till the network "learns" to "understand" the relationship between input and output data. In the second phase, the trained network is put to test by simulating for an independent data set which is not used during the training phase.

TABLE III
NEURON INDEPENDENCE STUDY FOR CASE A

N_h	5	**10**	15	20	25	30	35	40
R	0.33	**0.49**	0.41	0.26	0.41	0.39	0.43	0.31

The newff library available with the commercial software package MATLAB R2010A is used as a tool for training and testing the network.

VI. RESULTS AND DISCUSSION

Major rain events observed in the tropical warm waters of the North Indian Ocean region bounded between 60° to 110° E and 0° to 25° N have been considered. During the period 2003 and 2010, 14 cyclones were observed and the TRMM satellite made 31 complete passes covering each of these cyclones in its various stages. The details of the cyclones and the TRMM orbit numbers are given in Table I.

The numerical weather model WRF is simulated to obtain pressure, temperature, relative humidity, cloud water mixing ratio, and rain water mixing ratio at 72 vertical levels of 250 m layer thickness. The initial conditions are chosen such that at time $T_{\rm ini} + \delta$ hours, the WRF simulations and TRMM overpass coincide, allowing us to collocate for the matching profiles. The time δ is chosen to be greater than 3 hours in order to allow the model to set in.

A. Retrieval of Near Surface Rain Rate From TMI Brightness Temperatures

Following the procedure explained in Section IV-A, the TMI and the TRMM PR pixels are collocated to determine the matching near surface rain rate for a given TMI pixel with nine brightness temperatures. A total of 6,711 matching profiles are identified, which is split into two sets; the first set of data consisting 5,034 profiles (∼75% of total data) is used to obtain the optimal weights of the network architecture, while the remaining 1,677 profiles are used to test the network learning efficiency.

A neuron independence study has been conducted in order to arrive at the number of hidden layer neurons $(\mathrm{N_h})$ enough to capture the relationship between the input and target values based on the correlation coefficient (R), and the results are presented in Table III.

From Table III, it can be seen that the architecture with 10 neurons in the hidden layer is correlated well compared to other architectures, and hence can be called as the "best" architecture.

Fig. 1 shows the scatter plot between TRMM PR near surface rain and the near surface rain simulated by the "best" neural network architecture.

Table III and Fig. 1 show that the best relationship between the two rain measuring instruments on board the TRMM satellite has a correlation of about 49% with an RMS error of about 10 mm/hr. This is because while the TRMM PR can detect only the precipitating particles, the TMI radiometer is sensitive to non-raining parameters such as water vapor and cloud particles, in addition to the rain parameters.

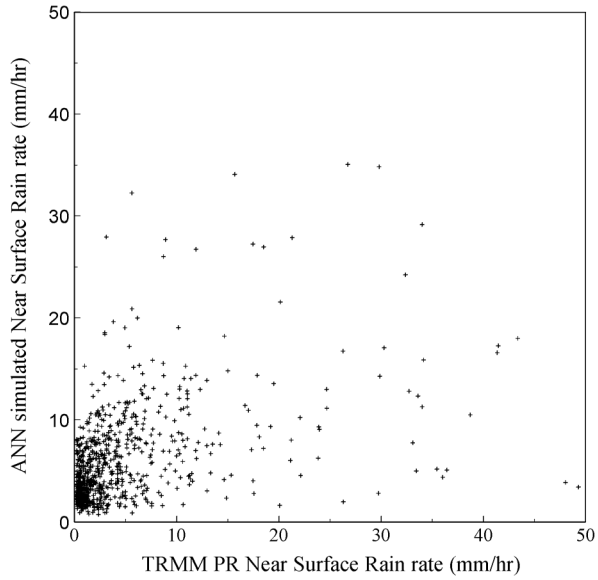

Fig. 1. Scatter plot of near surface rain measured by TRMM PR and neural network simulations.

B. Effect of Non-Raining Parameters on Retrieval of Surface Rainfall Simulated Using WRF From TMI BTs

A study has been conducted to see if inclusion of non-raining parameters in the training phase of the network improves the correlation between the near surface rain and the TMI brightness temperatures. For this, the WRF is used to simulate the rain mixing ratio (qr) and cloud mixing ratio (qc).

The WRF pixels are collocated with TRMM pixels as explained in Section IV-B and a matching database of 649 profiles is obtained. Of the 649 profiles, 487 profiles were used for training the neural network, while the remaining 162 are used to study the network performance.

The near surface rain rate (NSR) is calculated in two steps using the rain mixing ratio from the first two levels. In the first step, the rain mixing ratio at the first two levels from the surface is converted to rain contents using

$$W_r = (qr_1 + qr_2) \times \rho' \times 1000 \tag{14}$$

where ρ' refers to the density of humid air. The unit of W_r is g/m^3.

In the second step, the rain content is converted to rain rate following using the Marshall–Palmer distribution [18]

$$\mathrm{NSR} = 17.83 W_r^{1.19}$$

The cloud content (W_c) is calculated using the same formula given in (14) with qr being replaced with qc for all the 72 levels. The total cloud content is then calculated by integrating W_c along the vertical direction.

The total precipitable water content is obtained with an exactly similar approach, by vertically integrating the specific humidity at 72 TRMM PR levels. The near surface rain rate, the total cloud content and the total precipitable water content are now provided as inputs to the neural network.

TABLE IV
NEURON INDEPENDENCE STUDY FOR CASE B

N_h	**5**	10	15	20	25	30	35	40
R	**0.27**	0.17	0.1	0.05	0.2	0.21	0.11	0.03

During the training phase, the weights are updated iteratively to match with the TMI brightness temperatures that are collocated for each of the WRF profile. The results of the neuron independence study are shown in Table IV.

From Table IV, it can be seen that the addition of non-raining parameters has actually reduced the correlation coefficient from 0.49 to 0.27. One main reason for the worsening performance is that the numerical weather model outputs are generated using the same set of physics options for all the pixels which introduces errors in the data base.

C. Effect of Non-Raining Parameters on Retrieval of TRMM PR Near Surface Rain From TMI BTs

In order to minimize the error introduced by the WRF model, a study has been conducted by replacing the WRF simulated near surface rain (14) with TRMM PR's near surface rain obtained from 2A25 data products.

For the same 649 matching profiles obtained in Case B, the network is now trained with TRMM PR's near surface rain along with WRF simulated total cloud and precipitable water contents.

It has been found from the neuron independence study that five hidden neurons give better results compared to other architectures with a correlation coefficient of 0.53 and an RMS error of 8 mm/hr.

The result show that an improvement of about 4% correlation coefficient with the RMS error being reduced by about 2 mm/hr has been achieved by introducing the non-raining parameters while training the network for the simulation of rain rate.

D. Using TRMM PR Corrected Non-Raining Parameters to Improve the Estimation of Surface Rain Fall From TMI BTs

In this last case, a study is conducted to evaluate the use of TRMM PR corrected non-raining parameters simulated by WRF as inputs to the neural network. The corrections to the relative humidity, cloud and rain water mixing ratios are done in a Bayesian framework, using a non-commercial radar simulation package QuickBeam [19]. Fig. 2 shows the flowchart of the algorithm developed for Case D.

Two datasets are used in this case; the first data set (DS1) is used as an *a priori* database, while the second data set (DS2) is used for correcting the parameters. A total of about 1,000 WRF profiles were chosen in random in order to create an *a priori* database, while 524 WRF profiles that were collocated on TRMM pixels form dataset DS2. However, care has been taken to ensure that the profile represents various types of rainfall (low, medium, and high rainfall).

The *a priori* database containing WRF simulated pressure, temperature, relative humidity, cloud water mixing ratio, and rain water mixing ratio at 72 levels from DS1 forms the input of the radar simulation package QuickBeam.

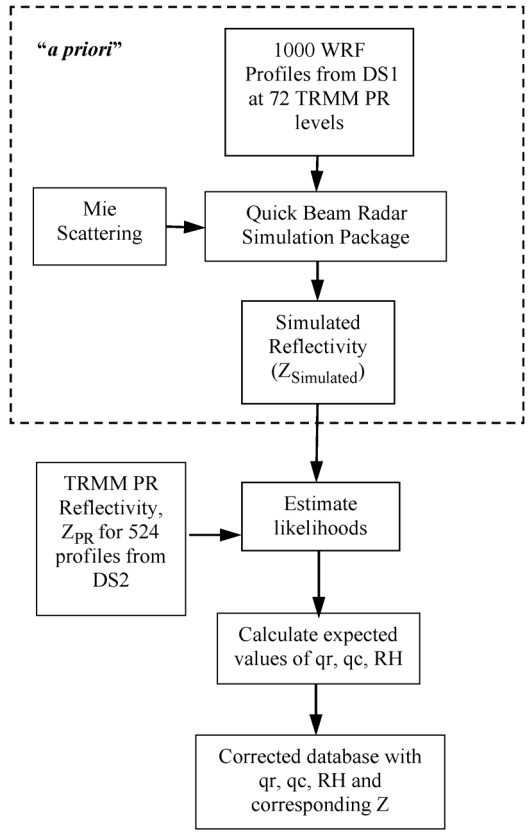

Fig. 2. Flowchart of profile correction algorithm for Case D.

For cloud and rain profiles, the drop size distribution is assumed to follow modified gamma distribution given by

$$N(d) = N_t \frac{1}{\Gamma(\upsilon) D_n} \left(\frac{D}{D_n}\right)^{\upsilon - 1} \exp\left(-\frac{D}{D_n}\right) \tag{16}$$

where

$$D_n = \overline{D} \frac{\Gamma(\upsilon + 1)}{\Gamma(\upsilon)}, \tag{17}$$

$\overline{D}$ is the mean diameter, equal to 1 μm for the cloud particles, and 1 mm for the rain. The width of the modified gamma distribution υ is assumed to be 4, following the PR 2A25 algorithm [20].

The cloud and rain drops are considered to be spherical in shape for which full Mie Scattering computations are performed and the reflectivity profiles are simulated by QuickBeam.

The simulated reflectivity profiles are then compared against a given TRMM PR reflectivity profile from DS2. The likelihood of each profile in the priori database is obtained by

$$w_j = \exp\left(-\sum_{i=1}^{72} \frac{(Z_{PR} - Z_i)^2}{2\sigma^2}\right) \tag{18}$$

TABLE V
NEURON INDEPENDENCE STUDY FOR CASE D

N_h	15	20	25	30	35	**40**
R	0.78	0.83	0.86	0.86	0.84	**0.88**

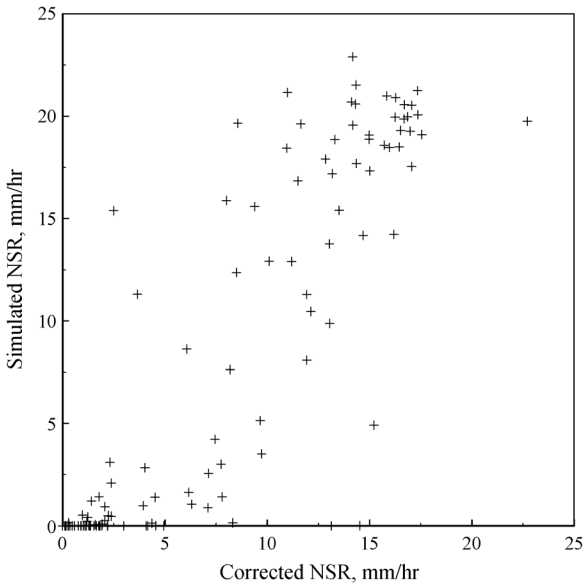

Fig. 3. Scatter plot of corrected near surface rain and neural network simulated rain rate.

where $1 \leq j \leq 1000$. The corrected profiles are obtained by calculating the expected value $E(X)$ as follows:

$$E(X) = \frac{\sum_{j=1}^{1000} w_j X_j}{\sum_{j=1}^{1000} w_j} \tag{19}$$

where X can be cloud mixing ratio, rain water mixing ratio, or relative humidity, as the case may be.

The corrected profiles in dataset DS2 are further split into two sets, first set of data with 393 profiles are used to train the neural network. The trained neural network is then tested for learning performance using the remaining 131 profiles. Table V shows the neuron independence study result for the case under consideration.

From Table V, it can be seen with the corrected WRF profiles, the non-raining parameters improved the correlation coefficient from 0.53 to 0.88 with a bias of 4 mm/hr.

Fig. 3 shows the scatter plot of the corrected near surface rain rate and the neural network simulated rain rate for the test data. It can be seen from Figs. 1 and 3 that addition of non-raining parameters has improved the training relationship with the brightness temperatures for various types of rainfall, low, medium, and high.

Fig. 4 shows the surface rainfall map simulated using the trained neural network for the cyclone Giri. Cyclone Giri was a very powerful tropical cyclone which caused huge loss of life and livestock of Myanmar in October 2010.

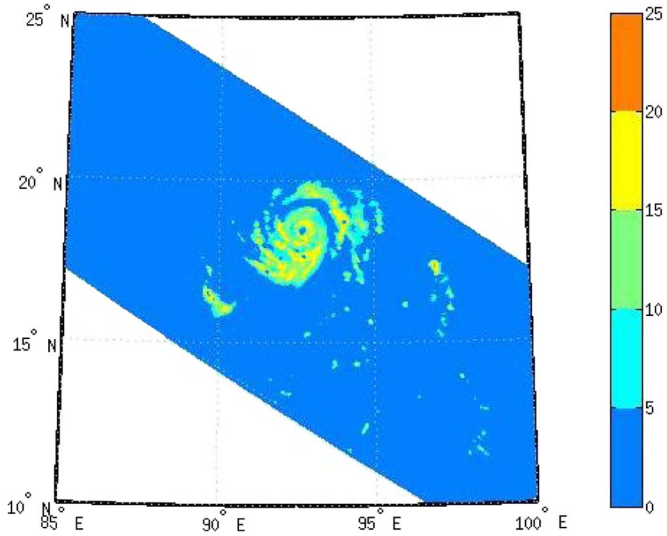

Fig. 4. Rainfall map simulated using neural network for cyclone Giri (rain rate in mm/hr).

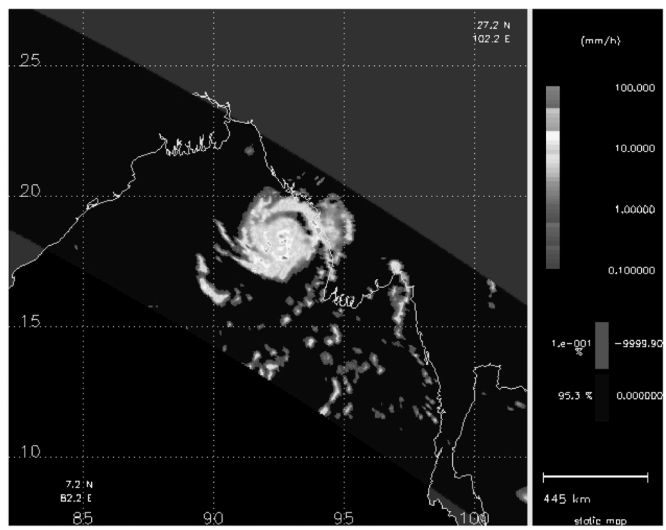

Fig. 5. Rainfall map from 2A12 database for cyclone Giri.

An area of low pressure was first identified on October 19, 2010. The system was developed into a depression the next day, and continued developing to reach its maximum intensity on October 22. At its peak, the maximum sustained wind speed was measured to be 165 km/h while the eye pressure was 950 hPa.

The TRMM satellite made an overpass of this cyclone on October 22, 2010 when the system was at its peak, and was about to make its landfall. TMI measured brightness temperatures from 1B11 data products is input to the neural network, while the output is the simulated rain rate in mm/hr.

It can be seen from Fig. 4 that the neural network is able to capture the low, medium and high rain rates. The neural network is also able to capture the "eye" of the cyclone. The surface rainfall map from 2A12 of TMI rain retrievals is shown in Fig. 5 for comparison.

Fig. 6 shows a map of the total cloud content in g/m^3 for the cyclone under consideration, an additional rain product that is

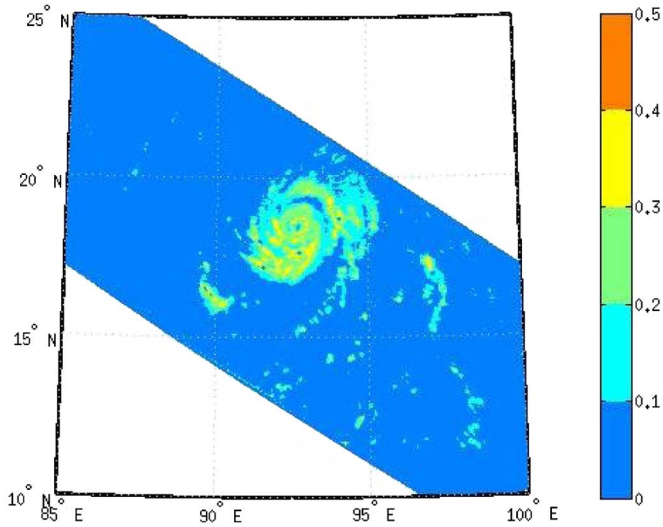

Fig. 6. Map of total cloud content ($\mathrm{kg/m^2}$) simulated by neural network.

an outcome of this study. The total cloud content, a key meteorological parameter, seems to have a good correlation with the rainfall map.

VII. Conclusions

The paper has discussed in detail the effect of non-raining parameters in retrieval of surface rain rate from passive microwave observations. A systematic study with a large database has been conducted to study the effect of total cloud and precipitable water contents on surface rainrate retrievals from the TMI measured brightness temperatures (BT) using neural networks.

Four cases were considered: (a) TRMM PR's near surface rain rate is correlated with TMI brightness temperatures; (b) the total cloud and precipitable water contents along with surface rainfall simulated using WRF are correlated with TMI BTs; (c) similar to case (b) with near surface rainfall taken from TRMM PR measurements; (d) total cloud and precipitable water contents and the surface rain rate are corrected with PR vertical reflectivity profile in a Bayesian framework. The freely available QuickBeam software was used for simulation of reflectivities at TRMM PR frequency.

Results show that for the case where the total cloud content and precipitable water simulated by WRF are used as input, the correlation coefficient improved from 0.49 to 0.53 with a reduction in the RMS error of 2 mm/hr when compared to a network trained with TRMM PR rain rate alone.

Further, when the WRF profiles are corrected in a Bayesian framework using TRMM PR reflectivities, the correlation coefficient increased dramatically from 0.53 to 0.88 with an RMS error of 4 mm/hr. The trained network can also be used for producing maps of total cloud content, a key meteorological parameter.

In summary, radar corrected hydrometeor structures generated from a mesoscale numerical weather prediction model, when correlated against radiometer brightness temperatures, result in a quantum jump in the quality of rainfall retrievals from microwave satellite radiances.

References

[1] C. Kummerow, W. Barnes, T. Kozu, J. Shiue, and J. Simpson, "The tropical rainfall measuring mission (TRMM) sensor package," *J. Atmosph. Ocean. Technol.*, vol. 15, pp. 809–817, 1998.

[2] F. S. Marzano, A. Mugnai, G. Panegrossi, and N. Pierdicca, "Bayesian estimation of precipitating cloud parameters from combined measurements of spaceborne microwave radiometer and radar," *IEEE Trans. Geosci. Remote Sens.*, vol. 37, pp. 596–613, Jan. 1999.

[3] H. Masunaga and C. Kummerow, "Combined radar and radiometer analysis of precipitation profiles for a parametric retrieval algorithm," *J. Atmosph. Ocean. Technol.*, vol. 22, pp. 909–929, Jul. 2005.

[4] M. Grecu and W. S. Olson, "Bayesian estimation of precipitation from satellite passive microwave observations using combined radar-radiometer retrievals," *J. Appl. Meteorol. Climatol.*, vol. 45, pp. 416–433, Mar. 2006.

[5] C. Kummerow, W. S. Olson, and L. Giglio, "A simplified scheme for obtaining precipitation and vertical hydrometeor profiles from passive microwave sensors," *IEEE Trans. Geosci. Remote Sens.*, vol. 34, no. 5, pp. 1213–1232, 1996.

[6] H. Czekala, S. Crewell, C. Simmer, and A. Thiele, "Discrimination of cloud and rain liquid water path by ground based polarized microwave radiometry," *Geophys. Res. Lett.*, vol. 28, pp. 267–270, 2001.

[7] G. D. Auria, F. S. Marzano, N. Pierdicca, P. Basili, and P. Ciotti, "Rain retrieval algorithms for passive microwave observations: A comparison and a choice," in *Proc. IGARSS'95*, Firenze, Italy, Jul. 10–14, 1995, pp. 1136–1137.

[8] E. A. Smith, A. Mugnai, H. J. Cooper, G. J. Tripoli, and X. Xiang, "Foundations for statistical-physical precipitation retrieval from passive microwave satellite measurements. Part I–Brightness-temperature properties of a time-dependent cloud-radiation model," *J. Appl. Meteorol.*, vol. 31, pp. 506–531, 1992.

[9] C. K. Bhattacharya and G. S. Uppal, "Determination of cloud liquid and precipitable water vapor by ground-based microwave radiometers," *IEEE Trans. Geosci. Remote Sens.*, vol. GRS-25, pp. 472–476, Jul. 1987.

[10] D. D. Turner, S. A. Clough, J. C. Liljegren, E. E. Clothiaux, K. E. Cady-Pereira, and K. L. Gaustad, "Retrieving liquid water path and precipitable water vapor from the atmospheric radiation measurement (ARM) microwave radiometers," *IEEE Trans. Geosci. Remote Sens.*, vol. 45, pp. 3680–3690, Nov. 2007.

[11] F. I. Sanchez, S. A. Boukabara, R. Chen, K. Garrett, C. Grassotti, W. Chen, and F. Weng, "Assessment of a variational inversion system for rainfall rate over land and water surfaces," *IEEE Trans. Geosci. Remote Sens.*, vol. 49, pp. 3311–3333, September 2011.

[12] J. A. Weinman, R. Meneghini, and K. Nakamura, "Retrieval of precipitation profiles from airborne radar and passive radiometer measurements: Comparison with dual-frequency radar measurements," *J. Appl. Meteorol.*, vol. 29, pp. 981–993, Oct. 1990.

[13] K. V. Ooyama, "A thermodynamic foundation for modeling the moist atmosphere," *J. Atmospher. Sci.*, vol. 47, pp. 2580–2593, 1990.

[14] W. C. Skamarock and J. B. Klemp, "A time-split nonhydrostatic atmospheric model for weather research and forecasting applications," *J. Computat. Phys.*, vol. 227, pp. 3465–3485, 2008.

[15] W. C. Skamarock, J. B. Klemp, J. Dudhia, D. O. Gill, D. M. Barker, W. Wang, and J. G. Powers, "A description of the advanced research WRF," version 2, NCAR/TN-468+STR National Center for Atmospheric Research, NCAR Technical Note, 2007.

[16] R. Chandrasekar and C. Balaji, "Sensitivity of tropical cyclone Jal simulations to physics parameterizations," *J. Earth Syst. Sci.*, (in press).

[17] Tropical Rainfall Measuring Mission (TRMM) data products. Mirador, Goddard Earth Sciences Data and Information Services Ctr., May 2, 2011 [Online]. Available: http://mirador.gsfc.nasa.gov/cgi-bin/mirador/presentNavigation.pl?tree=project&project=TRMM&dataGroup=Orbital

[18] J. Marshall and W. Palmer, "The distribution of raindrops with size," *J. Atmosph. Sci.*, vol. 5, no. 4, pp. 165–166, 1948.

[19] J. M. Haynes, R. T. Marchand, Z. Luo, A. Bodas-Salcedo, and G. L. Stephens, "A multipurpose radar simulation package: QuickBeam," *Bulletin of the American Meteorological Society*, 10.1175/BAMS-88-11-1723.

[20] T. Iguchi, T. Kozu, R. Meneghini, J. Awaka, and K. Okamoto, "Rain-profiling algorithm for the TRMM precipitation radar," *J. Appl. Meteorol.*, vol. 39, pp. 2038–2052, December 2000.

Srinivasa Ramanujam received the B.E degree in mechanical engineering from Madras University, India, in 2003, and the M.S. degree in engineering from SASTRA University, India, in 2008. He is currently working toward the Ph.D. degree at IIT Madras.

His area of research is inverse problems in satellite remote sensing.

Chandrasekar Radhakrishnan received the B.E. degree in mechanical engineering from Anna University, India, in 2006, and the M.E degree in heat power engineering from Coimbatore Institute of Technology, India, in 2009. He is currently working toward the Ph.D. degree at IIT Madras.

His area of research is impact of data assimilation techniques in numerical weather forecasting.

Deepak Subramani is currently pursuing the Bachelors and Masters Dual Degree program in mechanical engineering at the Indian Institute of Technology Madras.

Balaji Chakravarthy received the B.E. degree in mechanical engineering from Anna University, India, in 1990. He received the M.Tech. and Ph.D. degrees in heat transfer from IIT Madras, India, in 1992 and 1995, respectively.

After his Ph.D. he joined the National Institute of Technology Trichy as a Lecturer. After two years, he joined the National Institute of Ocean Technology (NIOT), India, as a visiting scientist in 1996, and became a Senior Project Manager at NIOT in 1998. He joined IIT Madras as an Assistant Professor in 1998 and became a Professor in 2009. His current research is application of optimization techniques in heat transfer and atmospheric sciences.